# Analytical Model for Calculation of Current Density Distributions over Cross-Section of a Multi-Conductor Cable

***Karlo Q. da Costa[1], Victor Dmitriev[1], João T. Pinho[1], Sérgio Colle[2], Luciana Gonzalez[1], Marcelo A. Andrade[3], João C. V. da Silva[3], Mauro Bedia[3]***

[1]Department of Electric Engineering / Federal University of Pará
Belém – Pará – Brazil
+55-91-32111299 ·karlo@ufpa.br
[2]Department of Mechanical Engineering / Federal University of Santa Catarina
Florianópolis – Santa Catarina – Brazil
+55-48-32342161 ·colle@emc.ufsc.br
[3]Prysmian Telecomunicações Cabos e Sistemas do Brasil S.A.
Sorocaba – São Paulo – Brazil
+55-15-32359209 · marcelo.andrade@prysmian.com

## Abstract

This work presents an analytical model based on Maxwell's equations for current density and electromagnetic field structure calculations in multi-conductor cables. One example of such cables is a composite fiber-optic overhead ground wire (OPGW). A circular multilayer waveguide model is used to represent approximately this cable. The waveguide consists of four layers: dielectric (silica) in the core, aluminum in the intermediate layer, steel in the outer layer and air. We analyze analytically $TM^z_{0n}$ modes of the waveguide which have axial symmetry. The numerical results presented here are the dispersion characteristics, the distribution of the electromagnetic fields and the variation of the current density in the cross-section of the waveguide as a function of frequency. This model allows one in particular to investigate the skin effect and the electromagnetic fields inside and outside of the cable.

**Keywords:** OPGW, waveguide model, current density, dispersion characteristics, electromagnetic fields, skin effect.

## 1. Introduction

The multi-conductor cable OPGW is used with the double function: of lightning protection for high voltage transmission lines, and as a communications channel through the optical fibers embedded in the cable structure. The optical fiber package is protected by an aluminum tube, which is covered by wires made of steel or steel-aluminum weld. When submitted to short-circuited or lightning conditions, several factors, such as caging, plastic deformations in the tube, disruption and/or destruction of the armored steel wires, determine damage effects in such cables, which could compromise the cable integrity. The calculation of heat distribution in the cross-section of a cable [1] is based on the distribution of current density, which in its turn, depends on the skin effect. Knowing the current pulse in the cable, one can calculate the spectrum of the pulse, and consequently, the range of frequencies where the most part of the electric power is concentrated. The following analysis of the current density distribution therefore can be fulfilled in the frequency domain. We present in this paper an electrodynamic model of a multiconductor OPGW cable. This model is used for analysis of current density and electromagnetic field distribution in the cable. In our model, the real cable is substituted by a multilayer structure consisting of a dielectric rod, an intermediate aluminum layer and an outer layer of steel. In contrast to earlier publications [2,3], in our analysis we do not introduce the approximation: "in metals, conduction current is much more greater than the displacement current", and this allows us to analyze a wider class of electromagnetic problems.

## 2. Mathematical Model

The cross section geometry of the OPGW cable and the corresponding waveguide model are shown in Fig. 1a and Fig.1b, respectively. The model consists of four homogeneous layers: dielectric ($\rho<a$), aluminum ($a<\rho<b$), steel ($b<\rho<c$), and air ($\rho>c$). The metal layers under consideration have finite conductivities. The analysis of the waveguide is based on Maxwell's equations in the frequency domain. As a first step, we consider the eigenvalue problem. We shall look for the electromagnetic fields $TM^z_{0n}$ and the currents which do not have variations with respect to the azimuthal coordinate $\phi$, i.e. $\partial/\partial\phi=0$ and $n$ is a nonnegative integer.

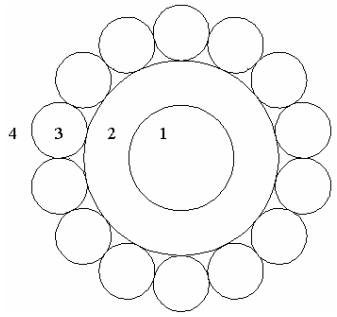


(a)

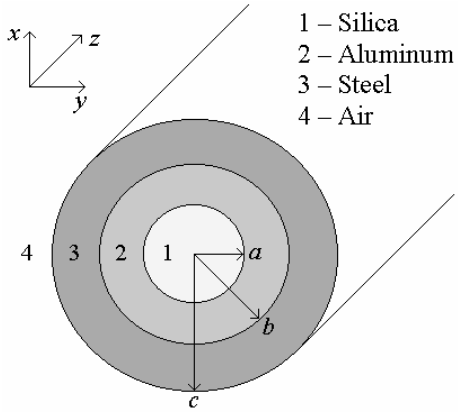


(b)

**Figure 1. Cross section geometry of the OPGW cable. (a) real geometry. (b) geometry of the analytical model.**

## 2.1 General electromagnetic fields solutions

From the Maxwell equations in cylindrical coordinate system in the frequency domain, the set of equations for TM$^z$ modes for the layers 1-4 shown in Fig. 1 is given by

$$\frac{\partial E_\rho}{\partial z} - \frac{\partial E_z}{\partial \rho} = -j\omega\mu H_\phi \tag{1}$$

$$\frac{\partial H_\phi}{\partial z} = -j\omega\varepsilon E_\rho \tag{2}$$

$$\frac{1}{\rho}\frac{\partial(\rho H_\phi)}{\partial \rho} = j\omega\varepsilon E_z \tag{3}$$

where $\omega=2\pi f$ is the angular frequency, $f$ is the frequency in Hz, $\mu$ and $\varepsilon$ are, respectively, the magnetic permeability and the electric permittivity of the layers under consideration (Fig. 1b). Using $\exp(-jk_z z)$ dependence of the electromagnetic fields, we obtain the following system of equations:

$$E_\rho(\rho,z) = E_\rho(\rho)e^{-jk_z z} \tag{4}$$

$$E_z(\rho,z) = E_z(\rho)e^{-jk_z z} \tag{5}$$

$$H_\phi(\rho,z) = H_\phi(\rho)e^{-jk_z z} \tag{6}$$

Using the fields in (1)-(3), the following equations are obtained

$$-jk_z E_\rho - \frac{\partial E_z}{\partial \rho} = -j\omega\mu H_\phi \tag{7}$$

$$E_\rho = \frac{k_z}{\omega\varepsilon} H_\phi \tag{8}$$

$$E_z = \frac{1}{j\omega\varepsilon}\frac{1}{\rho}\frac{\partial(\rho H_\phi)}{\partial \rho} \tag{9}$$

Substituting (8-9) in (7), we obtain the following differential equation:

$$\frac{d}{d\rho}\left[\frac{1}{\rho}\frac{d(\rho H_\phi)}{d\rho}\right] + \gamma^2 H_\phi = 0 \tag{10}$$

where $\gamma^2 = k^2 - k_z^2 = \omega^2\mu\varepsilon - k_z^2$. Substituting $x=\gamma\rho$ in this equation we come to the Bessel equation

$$\frac{d^2 H_\phi}{dx^2} + \frac{1}{x}\frac{dH_\phi}{dx} + \left(1 - \frac{1}{x^2}\right)H_\phi = 0 \tag{11}$$

with the possible solutions in the form of Bessel, Hankel and modified Bessel functions. The general solutions for the fields $H_\varphi$ and $E_z$ in layers 1-4 are written in Table 1.

Table 1: General field solutions $E_z$ and $H_\phi$ of the waveguide.

| | Fields (eigenfunctions) | Eigenvalue and constant of propagation |
|---|---|---|
| 1 | $\begin{cases} H_{\phi 1} = C_1 J_1(\gamma_1\rho) \\ E_{z1} = \dfrac{C_1\gamma_1}{j\omega\varepsilon_1} J_0(\gamma_1\rho) \end{cases}$ | $\gamma_1^2 = k_1^2 - k_z^2$<br>$k_1 = \omega\sqrt{\mu_0\varepsilon_1}$<br>$= \omega\sqrt{\mu_0\varepsilon_0\varepsilon_{r1}}$ |
| 2 | $\begin{cases} H_{\phi 2} = C_2 J_1(\gamma_2\rho) + C_3 Y_1(\gamma_2\rho) \\ E_{z2} = \dfrac{\gamma_2}{j\omega\varepsilon_2}[C_2 J_0(\gamma_2\rho) + C_3 Y_0(\gamma_2\rho)] \end{cases}$ | $\gamma_2^2 = k_2^2 - k_z^2$<br>$k_2 = \omega\sqrt{\mu_0\varepsilon_2}$<br>$= \omega\sqrt{\mu_0\left(\varepsilon_0\varepsilon_{r2} + \dfrac{\sigma_2}{j\omega}\right)}$ |
| 3 | $\begin{cases} H_{\phi 3} = C_4 J_1(\gamma_3\rho) + C_5 Y_1(\gamma_3\rho) \\ E_{z3} = \dfrac{\gamma_3}{j\omega\varepsilon_3}[C_4 J_0(\gamma_3\rho) + C_5 Y_0(\gamma_3\rho)] \end{cases}$ | $\gamma_3^2 = k_3^2 - k_z^2$<br>$k_3 = \omega\sqrt{\mu_0\varepsilon_3}$<br>$= \omega\sqrt{\mu_0\left(\varepsilon_0\varepsilon_{r3} + \dfrac{\sigma_3}{j\omega}\right)}$ |
| 4 | $\begin{cases} H_{\phi 4} = C_6 H_1^{(2)}(\gamma_4\rho) \\ E_{z4} = \dfrac{C_6\gamma_4}{j\omega\varepsilon_4} H_0^{(2)}(\gamma_4\rho) \end{cases}$ | $\gamma_4^2 = k_4^2 - k_z^2$<br>$k_4 = \omega\sqrt{\mu_0\varepsilon_0} = \omega\sqrt{\mu_0\varepsilon_1}$ |

In this table, the parameters $\mu_0$ and $\varepsilon_0$ are respectively the magnetic permeability and the electric permittivity of the free space, $\varepsilon_1$- $\varepsilon_3$ the electric permittivity of the layers 1-3, $\varepsilon_{r1}$- $\varepsilon_{r3}$ the relative electric permittivity of the layers 1-3, and $\sigma_2$ and $\sigma_3$ the electric conductivity of the layers 2 and 3. The constants $C_2$-$C_6$ can be expressed in terms of $C_1$.

## 2.2 Eigenvalue equation

The eigenvalue equation to determine the parameters $\gamma_1$- $\gamma_4$ presented in Table 1 is derived in this section. Note that the parameters $\gamma_1$- $\gamma_4$ are related to each other, for example $\gamma_2^2 = \gamma_1^2 + k_2^2 - k_1^2$. Thus we can calculate only one of them, and the others will be automatically determined. The parameter chosen in our analysis is $\gamma_1$. The procedure to obtain the eigenvalues equation is as follows.

Using the general solutions presented in Table 1 and applying the boundary conditions of continuity of the fields $E_z$ and $H_\phi$ at the surfaces $\rho=a$, $\rho=b$ and $\rho=c$, the following set of equations is obtained

$$C_1 J_1(\gamma_1 a) = C_2 J_1(\gamma_2 a) + C_3 Y_1(\gamma_2 a) \tag{12}$$

$$C_2 J_1(\gamma_2 b) + C_3 Y_1(\gamma_2 b) = C_4 J_1(\gamma_3 b) + C_5 Y_1(\gamma_3 b) \tag{13}$$

$$C_4 J_1(\gamma_3 c) + C_5 Y_1(\gamma_3 c) = C_6 H_1^{(2)}(\gamma_4 c) \tag{14}$$

$$\frac{C_1\gamma_1}{j\omega\varepsilon_1} J_0(\gamma_1 a) = \frac{\gamma_2}{j\omega\varepsilon_2}[C_2 J_0(\gamma_2 a) + C_3 Y_0(\gamma_2 a)] \tag{15}$$

$$\frac{\gamma_2}{j\omega\varepsilon_2}[C_2 J_0(\gamma_2 b) + C_3 Y_0(\gamma_2 b)] = \frac{\gamma_3}{j\omega\varepsilon_3}[C_4 J_0(\gamma_3 b) + C_5 Y_0(\gamma_3 b)] \tag{16}$$

$$\frac{\gamma_3}{j\omega\varepsilon_3}[C_4 J_0(\gamma_3 c) + C_5 Y_0(\gamma_3 c)] = \frac{C_6\gamma_4}{j\omega\varepsilon_4} H_0^{(2)}(\gamma_4 c) \tag{17}$$

To simplify the notations, the following variables are defined

$$x_1 = J_1(\gamma_1 a),\ x_2 = J_1(\gamma_2 a),\ x_3 = Y_1(\gamma_2 a),\ x_4 = J_1(\gamma_2 b)$$

$$x_5 = Y_1(\gamma_2 b),\ x_6 = J_1(\gamma_3 b),\ x_7 = Y_1(\gamma_3 b),\ x_8 = J_1(\gamma_3 c)$$

$$x_9 = Y_1(\gamma_3 c),\ x_{10} = H_1^{(2)}(\gamma_4 c),\ x_{11} = \frac{\gamma_1}{j\omega\varepsilon_1} J_0(\gamma_1 a)$$

$$x_{12} = \frac{\gamma_2}{j\omega\varepsilon_2} J_0(\gamma_2 a),\ x_{13} = \frac{\gamma_2}{j\omega\varepsilon_2} Y_0(\gamma_2 a),\ x_{14} = \frac{\gamma_2}{j\omega\varepsilon_2} J_0(\gamma_2 b)$$

$$x_{15} = \frac{\gamma_2}{j\omega\varepsilon_2} Y_0(\gamma_2 b),\ x_{16} = \frac{\gamma_3}{j\omega\varepsilon_3} J_0(\gamma_3 b),\ x_{17} = \frac{\gamma_3}{j\omega\varepsilon_3} Y_0(\gamma_3 b)$$

$$x_{18} = \frac{\gamma_3}{j\omega\varepsilon_3} J_0(\gamma_3 c),\ x_{19} = \frac{\gamma_3}{j\omega\varepsilon_3} Y_0(\gamma_3 c),\ x_{20} = \frac{\gamma_4}{j\omega\varepsilon_4} H_0^{(2)}(\gamma_4 c) \tag{18}$$

Replacing (18) in (12)-(17), we obtain the following system of linear equations:

$$\begin{bmatrix} x_1 & -x_2 & -x_3 & 0 & 0 & 0 \\ 0 & x_4 & x_5 & -x_6 & -x_7 & 0 \\ 0 & 0 & 0 & x_8 & x_9 & -x_{10} \\ x_{11} & -x_{12} & -x_{13} & 0 & 0 & 0 \\ 0 & x_{14} & x_{15} & -x_{16} & -x_{17} & 0 \\ 0 & 0 & 0 & x_{18} & x_{19} & -x_{20} \end{bmatrix} \begin{bmatrix} C_1 \\ C_2 \\ C_3 \\ C_4 \\ C_5 \\ C_6 \end{bmatrix} = \begin{bmatrix} 0 \\ 0 \\ 0 \\ 0 \\ 0 \\ 0 \end{bmatrix} \tag{19}$$

It can be written compactly as $[x]\times[C]=[0]$. The constants $C_2$-$C_6$ can be expressed in terms of $C_1$:

$$C_2 = C_1 \frac{(x_1 x_{13} - x_3 x_{11})}{x_2 x_{13} - x_{12} x_3} \tag{20}$$

$$C_3 = C_1 \frac{(x_2 x_{11} - x_1 x_{12})}{x_2 x_{13} - x_{12} x_3} \tag{21}$$

$$C_4 = \frac{d_1 x_{17} - d_2 x_{17}}{x_6 x_{17} - x_{16} x_7} \tag{22}$$

where $d_1 = C_2 x_4 - C_3 x_5$ and $d_2 = C_2 x_{14} - C_3 x_{15}$

$$C_5 = \frac{d_2 x_6 - d_1 x_{16}}{x_6 x_{17} - x_{16} x_7} \tag{23}$$

$$C_6 = \frac{C_4 x_8 - C_5 x_9}{x_{10}} \tag{24}$$

The system (19) possesses nontrivial solution if and only if the determinant of $[x]$ is null, i.e.

$$\det[x]=0 \tag{25}$$

This is the eigenvalue equation and the solution of it gives the eigenvalue $\gamma_1$. The parameters $\gamma_2$- $\gamma_4$ expressed as functions of $\gamma_1$ are

$$\gamma_2^2 = \gamma_1^2 + \omega^2\mu_0(\varepsilon_2 - \varepsilon_1) \tag{26}$$

$$\gamma_3^2 = \gamma_1^2 + \omega^2\mu_0(\varepsilon_3 - \varepsilon_1) \tag{27}$$

$$\gamma_4^2 = \gamma_1^2 + \omega^2\mu_0(\varepsilon_4 - \varepsilon_1) \tag{28}$$

In order to solve (25), the following normalizations of (26)-(28) are used:

$$\gamma_1 a = \xi \tag{29}$$

$$\gamma_2 a = \sqrt{\xi^2 + (k_0 a)^2(\varepsilon_{R2} - \varepsilon_{r1})} \tag{30}$$

$$\gamma_2 b = \left(\frac{b}{a}\right)\sqrt{\xi^2 + (k_0 a)^2(\varepsilon_{R2} - \varepsilon_{r1})} \tag{31}$$

$$\gamma_3 b = \left(\frac{b}{a}\right)\sqrt{\xi^2 + (k_0 a)^2(\varepsilon_{R3} - \varepsilon_{r1})} \tag{32}$$

$$\gamma_3 c = \left(\frac{c}{a}\right)\sqrt{\xi^2 + (k_0 a)^2(\varepsilon_{R3} - \varepsilon_{r1})} \tag{33}$$

$$\gamma_4 c = \left(\frac{c}{a}\right)\sqrt{\xi^2 + (k_0 a)^2(\varepsilon_{R4} - \varepsilon_{r1})} \tag{34}$$

where $k_0 = \omega\sqrt{\mu_0\varepsilon_0} = k_4$, $\varepsilon_{R2} = \varepsilon_{r2} + \sigma_2 / j\omega\varepsilon$, $\varepsilon_{R3} = \varepsilon_{r3} + \sigma_3 / j\omega\varepsilon$, and $\varepsilon_{R4}$=1. Substituting (29)-(34) in (25), the resulting equation becomes a function of $\xi$. As the elements of the matrix $[x]$ are complex, the solutions $\xi$ are also complex numbers, with the real part $\xi_r$ and the imaginary part $\xi_i$. With these notations, (25) is a system of two equations and two unknowns $\xi_r$ and $\xi_i$.

$$\begin{cases} F_1(\xi_r, \xi_i) = \mathrm{Re}(\det[x]) = 0 \\ F_2(\xi_r, \xi_i) = \mathrm{Im}(\det[x]) = 0 \end{cases} \tag{35}$$

The solutions of (35) are the points where the curves $F_1$ and $F_2$ are crossed.

## 3. Numerical results and discussions

To solve the system (35), a computer code in the software Matlab was developed. Using this program, eigenvalues $\gamma_1$ of the modes $TM^z$, the electromagnetic fields and currents can be calculated. The input data in this code are the electromagnetic and geometric parameters of the waveguide and frequency.

In order to verify the developed code, the following two sections present the results of calculations for two waveguides with the known solutions: the circular metallic waveguide and the circular dielectric waveguide. They are particular cases of the four-layer structure. Some numerical results obtained for OPGW cables will be presented in Section 3.3.

### 3.1 Circular metallic waveguide

The simulation of this waveguide by the developed software can be done choosing the values of the radius $b$ and $c$ close to the radius $a$, and setting a perfect dielectric in the region 1 (Fig. 1b). One simulation was performed for this waveguide. The parameters of the waveguides used in the simulation are given in Table 2.

Fig. 2 shows the $F_1$ and $F_2$ curves obtained for the simulation (Table 2), and the Fig. 3 shows the variation of $K_z/K_0$ versus $2a/\lambda_0$ ($\lambda_0$ is the wavelength in free space) for two modes.

Table 2: Input data of the simulation of the metallic waveguide.

| Region | $\varepsilon_r$ | $\sigma$(S/m) | Radius | Relative permittivity |
|---|---|---|---|---|
| 1 | 10 | 0 | $a$=0.5mm | 1 |
| 2 | 2 | $3.8\times10^7$ | $b$=0.55mm | 1 |
| 3 | 3 | $3.8\times10^7$ | $c$=0.6mm | 1 |
| 4 | 1 | 0 | - | 1 |

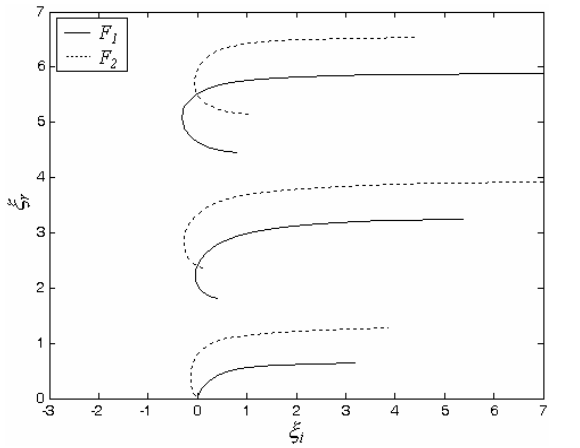


**Figure 2. Curves $F_1$ and $F_2$ obtained from simulation for the waveguide in Table 2.**

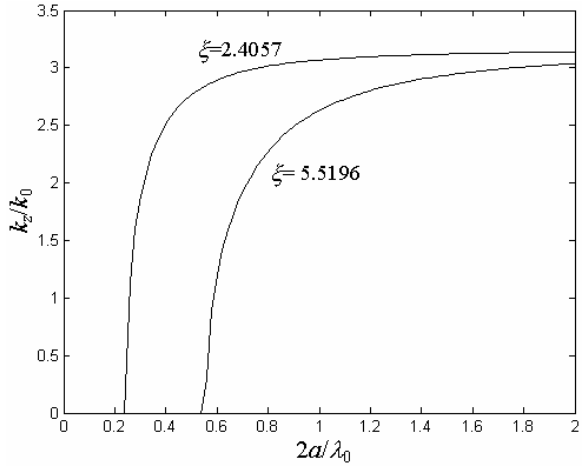


**Figure 3. Dispersion curves obtained from simulation for the waveguide in Table 2.**

Fig. 2 shows that in the range $0<\xi<7$, the eigenvalue solutions for the waveguide are $\xi$=0, 2.4057 and 5.5196. The second and the third eigenvalues are in concordance with the ideal circular metallic waveguide, but the value $\xi$=0 does not exist in the case of the ideal metallic waveguide. This eigenvalue appears due to the finite conductivity ($\sigma=3.8\times10^8$) of the metal, which produces finite electric field inside the conductors for low and medium frequency. This means that there is no cutoff frequency for this mode $TM^z$. In other words, in low frequencies only this mode propagates. In this work, this mode is called $TM^z_{00}$.

### 3.2 Circular dielectric waveguide

The simulation for this waveguide was done setting the values of the radius $b$ and $c$ close to the radius $a$, and setting a perfect dielectric on the layers 1-4, but with different relative permittivity (Fig. 1). The parameters used for calculations are given in Table 3. The obtained results are shown in Figs. 4-5. Again, our results coincide with the known ones.

Table 3: Input data of the simulation for dielectric waveguide.

| Region | $\varepsilon_r$ | $\sigma$(S/m) | Radius | Relative permittivity |
|---|---|---|---|---|
| 1 | 20 | 0 | $a$=0.5mm | 1 |
| 2 | 2 | 0 | $b$=0.505mm | 1 |
| 3 | 3 | 0 | $c$=0.51mm | 1 |
| 4 | 1 | 0 | - | 1 |

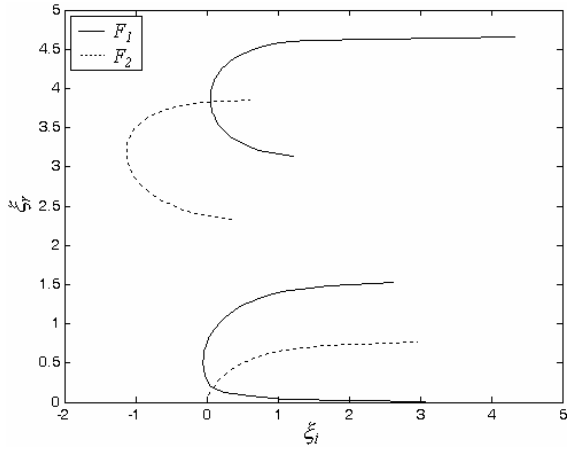


**Figure 4. Curves $F_1$ and $F_2$ obtained from simulation for the waveguide in Table 3.**

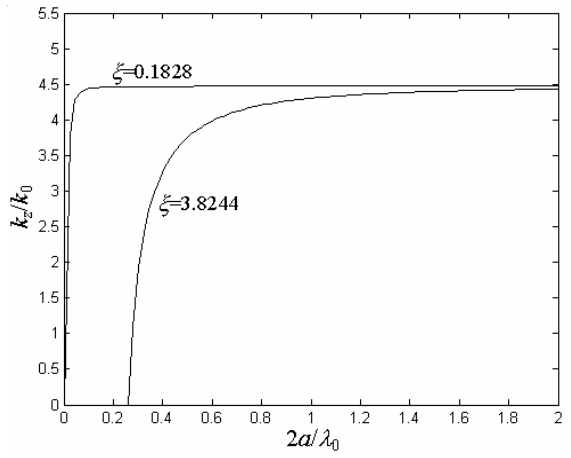


**Figure 5. Dispersion curves obtained from simulation 1 of the waveguide in Table 3.**

## 3.3 OPGW waveguide

The simulation of this waveguide was made using a perfect dielectric in the region 1 (Fig. 1), and the regions 2 and 3 as nonideal conductors. The materials used in the waveguide are shown in Fig. 1. The electromagnetic and geometric parameters are given in the Table 4.

Table 4: Input data for the simulation of the OPGW waveguide.

| Region | $\varepsilon_r$ | $\sigma$(S/m) | Radius | Relative permittivity |
|---|---|---|---|---|
| 1 | 3.8 | 0 | $a$=2.8mm | 1 |
| 2 | 1 | $3.96\times10^7$ | $b$=4.1mm | 1 |
| 3 | 1 | $0.2\times10^7$ | $c$=7.2mm | 1 |
| 4 | 1 | 0 | - | 1 |

### *3.3.1 Eigenvalues and dispersion curves*

Fig. 6 shows the calculated curves $F_1$ and $F_2$. The crossing points give the eigenvalues $\xi$=0, 1.3535, and 2.4065. Again, the mode $TM^z_{00}$ is present in this waveguide. Fig. 7 shows the dispersion curves obtained for the waveguide. Using this figure, it is possible to calculate the cutoff frequency corresponding to the eigenvalue $\xi$=1.3535. This value is 11.6 GHz, and the cutoff frequencies of the other superior modes are greater. For this reason, the only mode that propagates in low frequency is the $TM^z_{00}$. The next sections present the analysis of this mode.

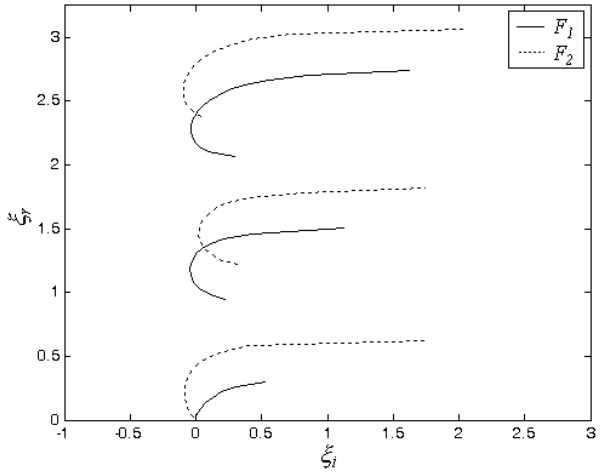


**Figure 6. Curves $F_1$ and $F_2$ obtained from simulation for the OPGW waveguide in Table 4.**

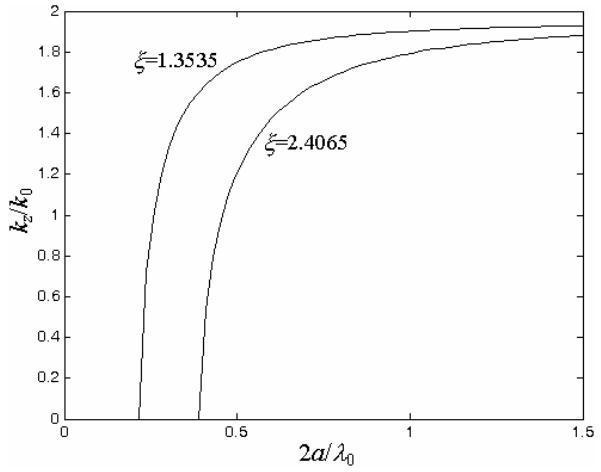


**Figure 7. Dispersion curves obtained from the simulation of the OPGW waveguide in Table 4.**

### *3.3.2 Electromagnetic field distribution*

Fig. 8 and 9 show the variation of the electric field $E_z$ versus radial coordinate $\rho$ for the frequencies 1, 5, 10, 50, 125, and 200 KHz. These curves show that when the frequency increases the electric field inside the waveguide diminishes. For the frequency 200 KHz, the skin depth $\delta$ is approximately 0.8mm.

The distribution of the magnetic field $H_\phi$ in function of $\rho$ for different frequencies is presented in Fig. 10 and 11. This field inside de waveguide is also reduced with increasing of the frequency.

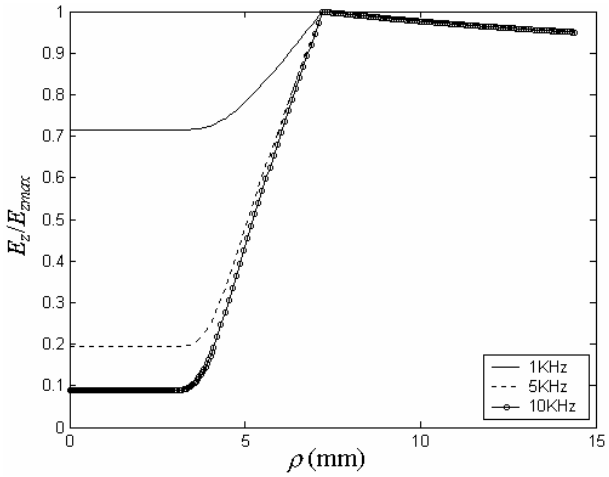


**Figure 8. Module of electric field $E_z$ versus radial coordinate.**

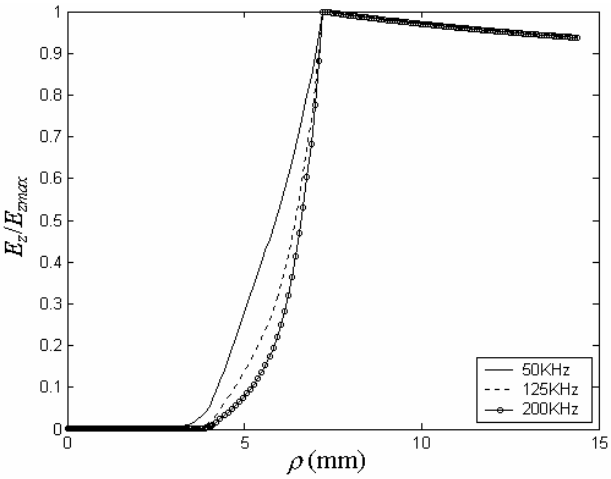


**Figure 9. Module of electric field $E_z$ in function of radial coordinate.**

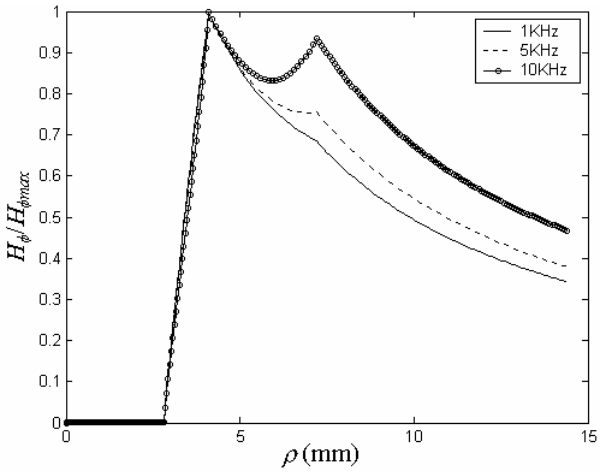


**Figure 10. Module of magnetic field $H_\phi$ in function of radial coordinate.**

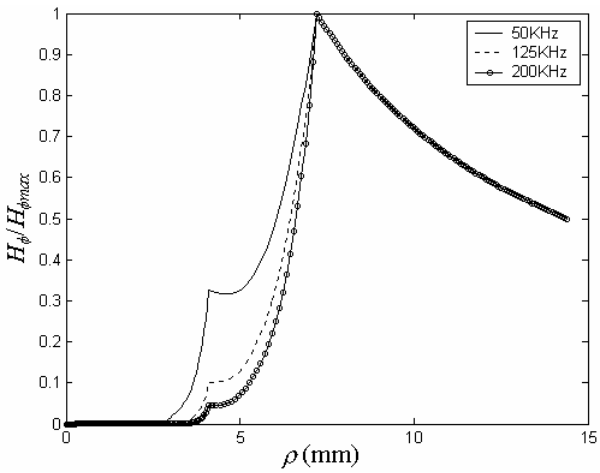


**Figure 11. Module of magnetic field $H_\phi$ in function of radial coordinate.**

### *3.3.3 Current density distributions*

The variation of the magnitude of the current density $J_z$ in function of radial coordinate $\rho$ of the waveguide is given in Fig. 12 and 13. These figures show the results calculated by our Matlab code and the commercial Finite Element Method Femlab software. The phase variation of this current density is presented in Fig. 14.

These results show that in the frequency 1 KHz and below this value, the current distribution is approximately constant in the conductive regions (2-3). In the low frequencies ($f$<1 KHz), there is no skin effect. In the frequency 5 KHz the skin effect appears. In 200 KHz, the current density practically exists only in the surface of the external conductor (surface of the steel layer). Fig. 14 shows that the phase of the current density $J_z$ has a larger variation in function of the $\rho$ when the frequency increases.

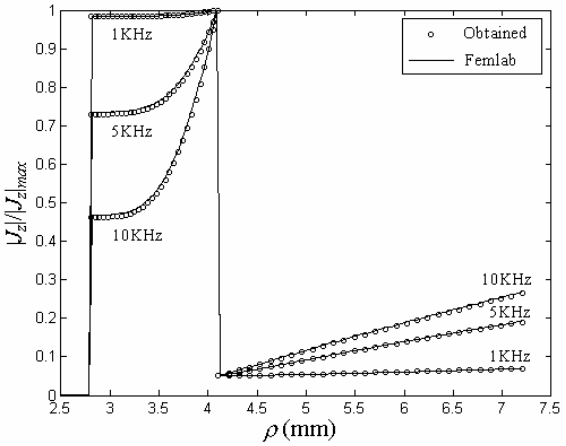


**Figure 12. Module of current density $J_z$ versus radial coordinate.**

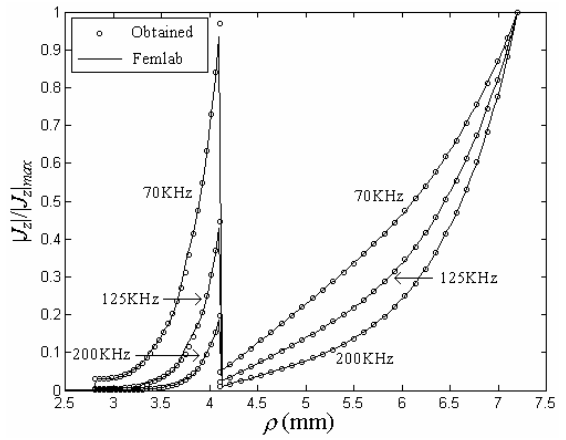


**Figure 13. Module of current density $J_z$ versus radial coordinate.**

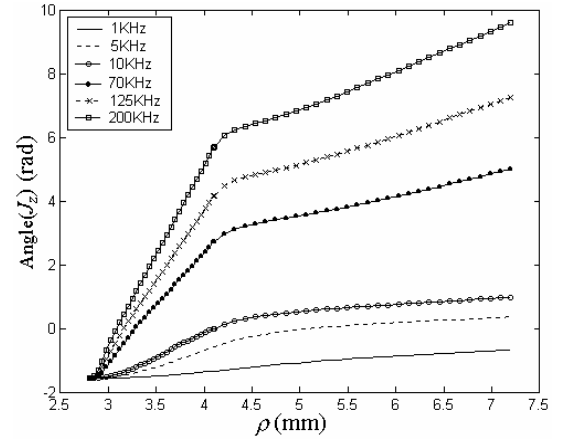


**Figure 14. Phase of current density $J_z$ versus radial coordinate.**

## 4. Conclusions

This paper presents an analytical model based on the exact solution of Maxwell's equations in frequency domain for analysis of multi-conductor cables. We have considered OPGW cable as a circular waveguide with four layers: dielectric, aluminum, steel and air.

The main results of our work are as follows. We developed an analytical waveguide model and computational program which allow one to calculate the electromagnetic field and current distributions in cables consisting of azimuthally uniform layers with nonideal materials, i.e. with metals with finite conductivity and dielectrics with losses. This model allows one, in particular to investigate the skin effect and the electromagnetic fields inside and outside of the cables.

The algorithm is verified by comparing with two known exact solutions of waveguide problems and with the solutions for current density distribution obtained by Finite Element Method using the commercial program Femlab.

## 5. References

[1] S. Colle, M. A. Andrade, J. T. Pinho, J. C. V. da Silva, M. Bedia, C. E. Veiga1, and J. N. Scussel, "Temperature Response of OPGW with Armored Aluminum Covered Steel Wires Submitted to Short-Circuit", accepted for publication in 2006 IWCS/Focus Conference.

[2] Z. Miro, J. Franc and T. Igor, "Skin effect impact on current density distribution in OPGW cables", Electrotechnical Review, Vol. 70, pp. 17 - 21, 2003.

[3] J. Franc, Z. Miro, T. Igor and U. Ivo, "Distribution of current density in layers of overhead bare conductors", Power System and Communications Infrastructures for the Future, Beijing, September 2002.

Karlo Queiroz da Costa was born in Belém, Pará, Brazil, on September 5, 1977. He received the B.Sc., M.Sc, and Dr. degree in electrical engineering from the Universidade Federal do Pará (Brazil) respectively in 2001, 2002, and 2006. He has joined with the Department of Electrical Engineering of the Federal University of Pará in 2006 as professor of applied electromagnetism.

His research interests are centered on applied electromagnetics, microwaves, antennas, propagation, numerical methods, and grounding systems. In these areas he has published many papers in conferences and periodicals.

Victor Dmitriev was born in Russia, in 1947. Currently, he is a professor at the Federal University of Para, Belem, Brazil. Dr. Victor Dmitriev has more than 120 papers in scientific journals, several books and patents. The fields of his scientific interest are microwave, millimeter wave and optic components, application of group theory to electromagnetic problems,

complex media, nanophotonics, and mathematical methods of electromagnetic theory.

João Tavares Pinho was born in Belém, Pará, Brazil, on August 22, 1955. He received the B.Sc. degree in electrical engineering from the Universidade Federal do Pará (Brazil) in 1977, the M.Sc. degree in electrical engineering from the Pontifícia Universidade Católica do Rio de Janeiro (Brazil) in 1984, and the Dr.-Ing. degree in electrical engineering from the Rheinisch-Westfälische Technische Hochschule Aachen (Germany) in 1990. He has been with the Department of Electrical Engineering of the Universidade Federal do Pará since 1978, has worked as an assistant at the RWTH Aachen, was the coordinator of the post-graduation course in electrical engineering at the UFPA from 1992 to 1994, and is presently a full professor and leader of a research group on energy alternatives and microwave applications.

His research interests have been centered on electromagnetics, especially on microwave applications, and on the application of hybrid systems for the generation of electricity, especially those involving photovoltaic and wind energy. In these areas he has supervised many graduate and undergraduate works and published several papers.

Prof. Pinho is ad hoc advisor for several committees and institutions in Brazil, member of various scientific societies, and presently president of the Brazilian Microwave and Optoelectronics Society, Vice-President for Membership Affairs of the International Solar Energy Society - Brazilian Section, and First Secretary of the Brazilian Solar Energy Association.

Prof. Sergio Colle

LEPTEN – Department of Mechanical Engineering – UFSC (Federal University of Santa Catarina)

88040-900 – Florianópolis – SC – Brazil
Bibliography:
Mechanical Engineer degree in 1970 - UFSC
Master of Science in Mechanical Engineering in 1972 – COPPE / University of Rio de Janeiro
Doctor of Science in Mechanical Engineering in 1976 – COPPE / University of Rio de Janeiro
Professor of Thermodynamics, Heat Transfer and Solar Energy – Department of Mechanical Engineering – UFSC since 1974
He is presently head of LEPTEN.

Luciana Pereira Gonzalez was born in Belém, Para, Brazil in 1977. She graduated in Electrical Engineering at the Federal University of Pará (UFPA) in May of 2006. She is now a postgraduate student at UFPA.

Marcelo de Araujo Andrade was born in Florianópolis – SC – Brazil in 1965. He graduated in Mechanical Engineer from Universidade Federal de Santa Catarina in 1988. He joined Prysmian Telecomunicações Cabos e Sistemas do Brasil in 1988 and actually he is in charge of Comercial and R&D Direction.

João Carlos Vieira da Silva was born in São Paulo – SP – Brazil in 1959. He graduated in BSc Physics from Universidade de São Paulo in 1982 and Electrical Engineer from Faculdade de Engenharia de Sorocaba in 1991. He joined Prysmian Telecomunicações Cabos e Sistemas do Brasil in 1977 and actually he is in charge of Product Engineering Department.

Mauro Bedia Jr. was born in São Paulo – SP – Brazil in 1970. He graduated in Mechanical Engineer from Faculdade Santa Cecília in 1996. He joined Prysmian Telecomunicações Cabos e Sistemas do Brasil in 1989 and actually he is responsible for OPGW and ADSS cable development.